Nitrate response of a lowland catchment: On the relation between stream concentration and travel time distribution dynamics

Y. van der Velde,[1,2] G. H. de Rooij,[3] J. C. Rozemeijer,[2,4] F. C. van Geer,[4,5] and H. P. Broers[2,5]

Received 14 January 2010; revised 27 August 2010; accepted 7 September 2010; published 20 November 2010.

[1] Nitrate pollution of surface waters is widespread in lowland catchments with intensive agriculture. For identification of effective nitrate concentration reducing measures the nitrate fluxes within catchments need to be quantified. In this paper we applied a mass transfer function approach to simulate catchment-scale nitrate transport. This approach was extended with time-varying travel time distributions and removal of nitrate along flow paths by denitrification to be applicable for lowland catchments. Numerical particle tracking simulations revealed that transient travel time distributions are highly irregular and rapidly changing, reflecting the dynamics of rainfall and evapotranspiration. The solute transport model was able to describe 26 years of frequently measured chloride and nitrate concentrations in the Hupsel Brook catchment (6.6 km^2 lowland catchment in the Netherlands) with an R^2 value of 0.86. Most of the seasonal and daily variations in concentrations could be attributed to temporal changes of the travel time distributions. A full sensitivity analysis revealed that measurements other than just surface water nitrate and chloride concentrations are needed to constrain the uncertainty in denitrification, plant uptake, and mineralization of organic matter. Despite this large uncertainty, our results revealed that denitrification removes more nitrate from the Hupsel Brook catchment than stream discharge. This study demonstrates that a catchment-scale lumped approach to model chloride and nitrate transport processes suffices to accurately capture the dynamics of catchment-scale surface water concentration as long as the model includes detailed transient travel time distributions.

Citation: van der Velde, Y., G. H. de Rooij, J. C. Rozemeijer, F. C. van Geer, and H. P. Broers (2010), Nitrate response of a lowland catchment: On the relation between stream concentration and travel time distribution dynamics, *Water Resour. Res.*, *46*, W11534, doi:10.1029/2010WR009105.

1. Introduction

[2] Catchments without real hillslopes, with an unconsolidated soil, a dense artificial drainage system, and high inputs of nutrients due to intensive agriculture, are found in deltas, river valleys, and plains worldwide. Polluted surface waters are an important environmental issue in all these catchments, with nutrient loads far exceeding loads in most mountainous catchments. Large-scale examples of relatively flat, densely drained agricultural plains causing nutrient pollution are the croplands in the Upper Mississippi River Basin implicated in the hypoxia in the Gulf of Mexico [*Petrolia and Gowda*, 2006] and the Pleistocene regions in the Netherlands whose discharge made shallow lakes turbid [*van der Molen et al.*, 1998].

[3] In lowland catchments, local groundwater head gradients toward ditches and tube drains are the driving force for water flow and solute transport [*Ernst*, 1978; *Raats*, 1977]. The dense artificial drainage systems create complicated dynamics in the spatial patterns of surface and subsurface fluxes of water and pollutants as they locally switch between active and passive depending on the ambient groundwater level [*van der Velde et al.*, 2009]. The measurements of *Wriedt et al.* [2007] and their simulations with a simplified two-dimensional flow model showed that temporal variations in groundwater heads and the resulting variations in groundwater flow route contributions can explain much of the observed dynamics in surface water nitrate concentrations. Thus, a hydrological model that accurately describes groundwater dynamics and the resulting fluxes of groundwater discharge, tube drain discharge, and overland flow is paramount to catchment-scale nitrate transport modeling. However, fully coupled water flow and solute transport models require many spatially distributed input parameters and are often tedious to operate at catchment scales for relevant spatial and temporal resolutions [*Kollet et al.*, 2010].

[1] Soil Physics, Ecohydrology and Groundwater Management Group, Wageningen University, Wageningen, Netherlands.
[2] Deltares, Utrecht, Netherlands.
[3] Department of Soil Physics, Helmholtz Centre for Environmental Research-UNZ, Halle, Germany.
[4] Department of Physical Geography, Utrecht University, Utrecht, Netherlands.
[5] TNO Geological Survey of the Netherlands, Utrecht, Netherlands.

0043-1397/10/2010WR009105

[4] A more conceptual approach was proposed by *Seibert et al.* [2009]. Their riparian profile flow-concentration integration model (RIM model) relates concentration depth profiles in the riparian zone to surface water concentrations. However, to scale up this point-scale concept to an entire lowland catchment, the dynamics of the active drainage network should be taken into account. A travel time distribution (TTD) approach, as introduced by *Rinaldo and Marani* [1987] under the term "mass transfer functions", and later refined by *Rinaldo et al.* [1989, 2006], relates flow routes to concentrations at basin scales. This approach is able to account for dynamic drainage networks if the TTD is allowed to change with time. The strengths of the TTD approach are that the approach is flow route based rather than location based, that it can be applied to large scales with only a few parameters, and that TTDs exist at any temporal and spatial scale [*Sivapalan*, 2003]. However, the current implementations of the TTD approach at basin scales [*Rinaldo et al.*, 2006; *Botter et al.*, 2005, 2008, 2009] have two major limitations. First, these studies assumed a constant TTD [*Rinaldo et al.*, 2006] or a combination of constant TTDs [*Botter et al.*, 2008, 2009] to characterize the hydrology of a catchment. In a recent study *Botter et al.* [2010] showed that constant TTDs do not exist, because the travel path and travel time of a water droplet are affected by rainfall and drought events during its journey through the catchment. Second, the TTD approach does not allow for spatial gradients of solutes. All previous catchment-scale transient studies using the TTD approach modeled a catchment as a completely mixed reservoir, which implies that all water droplets tend to the same equilibrium concentration independent of their location in the catchment. However, for nitrate, which is affected by denitrification, the groundwater concentration is often observed to decrease with depth or travel time [e.g., *Rozemeijer and Broers*, 2007; *Visser et al.*, 2009; *Zhang et al.*, 2009] and the TTD approach needs to be extended to include gradients along flow paths owing to denitrification.

[5] An alternative approach to quantify catchment-scale solute transport is by studying how a signal of rainfall concentrations is converted to stream concentrations, i.e., how solute concentrations in rainfall are filtered to generate solute concentrations at the catchment outlet. It appeared that small catchments may act as fractal filters [*Kirchner et al.*, 2000; *Cardenas*, 2007, 2008]. These catchment filter properties are a useful tool to compare solute transport between catchments, but they only allow for the derivation of the distribution of reaction times. This reaction time distribution describes the times it takes the concentration of a stream to react to a precipitation event. It does not necessarily describe the actual contact times of water parcels with the lithosphere of a catchment. Consequently, reaction time distributions are not suited for concentration calculations in a TTD approach as proposed by *Rinaldo et al.* [2006]. *Kollet and Maxwell* [2008] recognized the dynamic nature of TTDs. They used a particle tracking approach to calculate daily TTDs from a transient groundwater flow field and analyzed the resulting power spectra. However, they did not study the relation between transient TTDs and stream water quality dynamics.

[6] Of the approaches reviewed above, transient TTDs describing the various flow routes to the stream combined with concentration profiles along the flow paths offer the best opportunity to model both the rapid and slow variations in surface water concentrations that have often been observed [e.g., *Rozemeijer and Broers*, 2007]. The objectives of this paper are to extend the TTD approach for basin scales with transient TTDs and denitrification along flow paths, to quantify all nitrate fluxes and storages within a lowland catchment, and to assess to what extent temporal variations in TTDs can explain observed nitrate concentration changes.

[7] A common problem in nitrate transport modeling is that the unknown nitrate flux by denitrification causes large model uncertainty [*Haan and Skaggs*, 2003]. *Visser et al.* [2009] showed that this model uncertainty can partly be constrained by simultaneously solving the nitrate and chloride mass balances. If chloride (an inert, nondecaying tracer) and nitrate (a tracer with transport characteristics comparable to chloride but with denitrification) both mainly originate from agricultural inputs, the difference in behavior between chloride and nitrate can largely be attributed to denitrification. In this study we will adopt this approach of *Visser et al.* [2009] to partly constrain the uncertainty of the denitrification flux.

[8] First, we introduce a 26-year data set of nitrate and chloride measurements at the outlet of the Hupsel Brook catchment (6.6 km^2) during a period with declining agricultural inputs. Second, we derive a catchment-scale solute transport model combining elements of the solute transport at the basin-scale model [*Rinaldo et al.*, 2006; *Botter et al.*, 2005, 2008, 2009] and the RIM model [*Seibert et al.*, 2009]. This solute transport model is fed with transient travel time distributions derived by transient particle tracking and calibrated on measured surface water concentrations of nitrate and chloride. Third, a parameter sensitivity analysis is performed and the added value of transient TTDs is evaluated.

2. Materials and Methods

2.1. Study Area

[9] The Hupsel Brook catchment in the Netherlands has a long history as an experimental catchment and has been described extensively, for example, by *Wösten et al.* [1985], *Hopmans and Stricker* [1989], *van Ommen et al.* [1989], and *van der Velde et al.* [2009, 2010]. We offer a brief summary of the catchment characteristics and refer to the publications above for full details.

[10] The Hupsel Brook catchment (Figure 1) is situated in the eastern part of the Netherlands (52°06′N; 6°65′E). The size of the catchment is 6.64 km^2, with surface elevations ranging from 22 to 36 m above sea level. At depths ranging from 0.5 to 20 m, a 20–30 m thick impermeable marine clay layer of Miocene age is found. This clay layer forms a natural lower boundary for the unconfined groundwater flow [*van Ommen et al.*, 1989]. The unconfined aquifer consists of Pleistocene aeolian sands with occasional layers of clay, peat, and gravel of which the spatial extent is only marginally known. The average thickness of this aquifer is around 4 m, ranging from <1 to >20 m. *Wösten et al.* [1985] classified the main soil type of the catchment as a sandy, siliceous, mesic Typic Haplaquad (see *Wösten et al.* [1985] for more details).

[11] The Hupsel catchment is drained by a straightened and deepened main brook and by a dense artificial drainage network of ditches and tube drains. The spacing between the

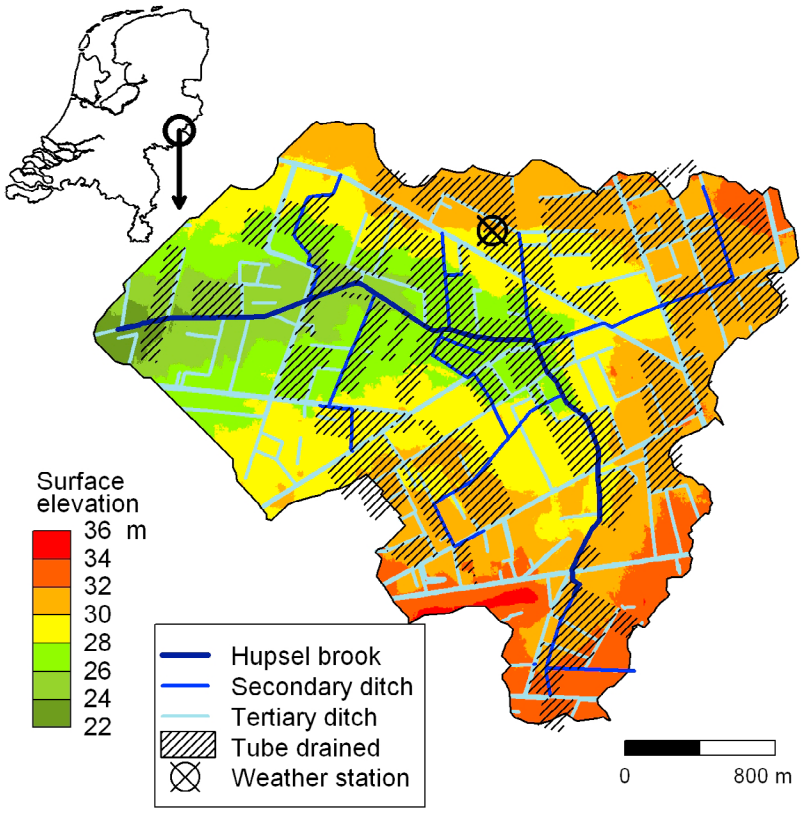

Figure 1. Hupsel Brook catchment.

ditches averages 300 m (Figure 1). Figure 1 also shows that tube drains were installed in approximately 50% of the agricultural fields in the catchment. The land use during past decades has predominantly been agricultural with maize and grassland. A few small patches of forest are located in the catchment. Residential areas are absent, but individual houses and farms are scattered throughout the area. None of these houses is allowed to discharge wastewater directly into the surface water network.

2.2. Collected Data for Period 1983–2008

2.2.1. Rainfall, Evapotranspiration, and Discharge

[12] The meteorological station of the Royal Dutch Meteorological Institute (KNMI) within the Hupsel Brook catchment has recorded hourly rainfall, incoming radiation, and temperature since 1993. For the period 1983–1992 we used data from a meteorological station located 28 km northeast of the catchment. The Makkink relation [*Makkink*, 1957], which requires incoming radiation and temperature, was applied to estimate daily potential evapotranspiration. Discharge records with an hourly resolution were available for the entire period.

2.2.2. Water Quality Measurements

[13] Chloride and nitrate concentrations at the Hupsel Brook catchment outlet have been measured since 1985. The first part of the data set was collected by an auto-sampler, taking average samples for every 5 mm of discharge (normalized by catchment area). This is the data period with the highest temporal resolution. From 1994 through 2003 the local water board took grab samples with an irregular time spacing (weeks to months). Finally, we collected weekly grab samples for May 2007 to December 2008.

2.2.3. Chloride and Nitrate Input Records

[14] Nitrate and chloride inputs to the catchment are mainly agricultural inputs of manure and fertilizer. Estimates of these inputs were adopted from the work of *van den Eerthwegh and Meinardi* [1999] for the period 1984–1993 and from the Centraal Bureau voor de Statistiek (CBS) Statline (http://statline.cbs.nl) for the period 1994–2007. All figures are regional estimates (260 km^2) for the total input of nitrate and chloride. Deviations of 20% or more can be expected for small catchments such as the Hupsel Brook catchment. Atmospheric inputs of nitrate (2–3 mg L^{-1}) and chloride (1–2 mg L^{-1}) were small compared to the large uncertainty in agricultural inputs and were not considered.

2.3. Solute Transport Model

[15] We developed a solute transport model for chloride and nitrate in lowland catchments. On the one hand, we wanted this model to cope with ephemeral active drainage systems which can be inferred from detailed topographic maps, soil type maps, and elevation data: properties that drive water transport [*van der Velde et al.*, 2009]. On the other hand, the model should include catchment-scale lumped expressions for solute transport by sorption, diffusion, denitrification, mineralization, and plant uptake

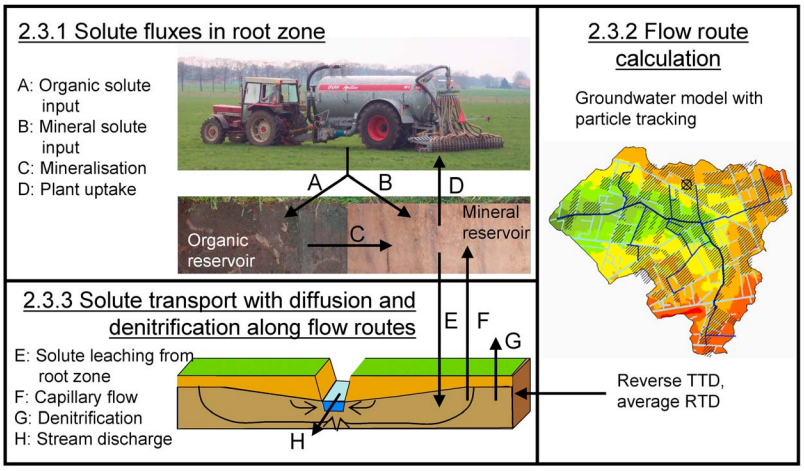

Figure 2. Schematic overview of the solute transport model. The headings indicate the sections of the main text detailing the model components.

reflecting the lack of spatial data for solute input, chemical soil parameters, soil heterogeneity, and plant-solute interactions. For clarity, we subdivided the model into three parts: (1) solute fluxes in the root zone, (2) catchment-scale flow route calculations within the saturated zone, and (3) solute transport with diffusion and denitrification along flow routes. The model is visualized in Figure 2. The boxes in Figure 2 represent the three parts. Definitions of the terms in Figure 2 will be given in sections 2.3.1 and 2.3.3.

2.3.1. Solute Fluxes in the Root Zone

[16] Within the root zone, mineralization of organic matter releases nitrate [*Hassink et al.*, 1993] and plants take up large amounts of nitrate and chloride. We accounted for these processes by introducing an organic reservoir and a mineral reservoir that both cover the entire catchment. We assumed that nitrate and chloride are only mobile in the mineral form: plant uptake, J_U [$M\ T^{-1}$], leaching from the root zone to the saturated zone, J_{leach} [$M\ T^{-1}$], and capillary flow from the saturated zone to the root zone, J_{cap} [$M\ T^{-1}$], can only occur with solutes in the mineral form (fluxes D, E, and F in Figure 2). The mass balances of the organic and mineral reservoirs are given by equations (1) and (2), respectively:

$$\frac{dW_{org}(t)}{dt} = (1-u_m)F(t) - r_m g_{\text{temp}}(t) W_{org}(t), \tag{1}$$

$$\frac{dW_{\min}(t)}{dt} = r_m g_{\text{temp}}(t) W_{org}(t) + u_m F(t) - J_U(t) - J_{\text{leach}}(t) + J_{cap}(t), \tag{2}$$

with

$$g_{\text{temp}}(t) = 0.1[\text{Temp}(t)] \text{ for Temp} > 0 \text{ and } g(t) = 0 \text{ for Temp} < 0. \tag{3}$$

The total solute mass stored in the organic reservoir is denoted by W_{org} [M], and that in the mineral reservoir is denoted by $W_{\min}$ [M]. The fertilizer and manure rate is denoted by F [$M\ T^{-1}$], and u_m is the fraction fertilizer in mineral form. Note that we assume that all chloride is applied in the mineral form ($u_{m\text{Cl}} = 1$). Consequently, chloride has no organic reservoir. The mineralization rate is denoted by r_m [T^{-1}] and is multiplied by a temperature coefficient g_{temp} (equation (3)) to capture the seasonal dynamics of mineralization [*Rodrigo et al.*, 1997]. Although many studies also report considerable effects of soil moisture on mineralization [e.g., *Herlihy*, 1979], we did not explicitly include soil moisture. The large spatial heterogeneity of soil moisture, the correlation between soil moisture and temperature, and the lack of measured mineralization rates did not justify a more complex model that includes soil moisture. The fertilizer and manure input, $F(t)$, is derived by distributing the yearly estimated input of chloride and nitrate uniformly over the period March–October, in line with Dutch regulations on manure applications. From November through February no fertilizer is applied. Note that no spatial variation in nitrogen and chloride application was taken into account, since we described the entire catchment with a single root zone reservoir.

[17] Plant uptake is considered proportional to the evapotranspiration flux, $E(t)$ [$L^3\ T^{-1}$]:

$$J_U(t) = \min(\text{Cu}E(t)\Delta t, W_{\min}(t))\Delta t^{-1}, \tag{4}$$

where Δt [T] is the length of the calculation time step. Because plants can regulate their uptake of solutes to a large extent, we defined a yearly average uptake concentration, Cu [$M\ L^{-3}$]. The minimum function (min) ensures that plants do not extract more than the available amount of solutes.

[18] Leaching of solutes from the root zone into the saturated zone is approximated by

$$J_{\text{leach}}(t) = \min\left(\max(P(t)-E(t),0)\frac{W_{\min}(t)}{\overline{S_{rz}}}\Delta t, W_{\min}(t) - J_U(t)\Delta t\right)\Delta t^{-1}, \tag{5}$$

where P(t) [$L^3\ T^{-1}$] is the rainfall flux over the entire catchment. The water flux that leaches through the root zone is assumed to be equal to the daily recharge:$\max(P(t) - E(t), 0)$. The term $W_{min}(t)/\overline{S_{rz}}$ is the average solute concentration in the root zone, where $\overline{S_{rz}}$ [L^3] is the temporally averaged

volume of water in the entire root zone of the catchment. The capillary flow of solutes from the saturated zone to the root zone, J_{cap}, is derived in section 2.3.3.

2.3.2. Catchment-Scale Flow Route Calculations Within the Saturated Zone

[19] Many studies have used travel time distributions (TTDs) to describe catchment-scale flow routes [*Rinaldo et al.*, 2006; *Botter et al.*, 2008; *Lindgren et al.*, 2004]. TTDs can be constructed for the input and the output fluxes of a flow volume. Because our main interest is in the concentration of the catchment-scale discharge, we will consider TTDs for the output, from here on named the reverse TTD and denoted by $f[T^{-1}]$. The reverse TTD at a particular time describes for how long the water parcels that contribute to the discharge at that time have been inside the catchment. The reverse TTD is the basis for the reverse transfer function model:

$$q_{\text{in}}(t) = \int_0^\infty f(T, t+T) q_{\text{out}}(t+T) dT, \tag{6}$$

where q_{in} is the influx and q_{out} is the outflux of water [$L^3\ T^{-1}$]; $f(T,t)$ [T^{-1}] is the contribution of travel time T to the total reverse TTD (the distribution of travel times water parcels spent inside the catchment) of the water discharged at time t. Transfer functions can be constructed for soil volumes as well as for entire catchments. Catchments, however, often have multiple exits for water as there is stream discharge, Q [$L^3\ T^{-1}$], evapotranspiration, E [$L^3\ T^{-1}$], and extraction by wells, O [$L^3\ T^{-1}$]. The reverse transfer function model for the catchment with multiple discharge routes is given by

$$P(t) = \int_0^\infty f_q(T, t+T) Q(t+T) dT + \int_0^\infty f_e(T, t+T) E(t+T) dT + \int_t^\infty f_o(T, t+T) O(t+T) dT, \tag{7}$$

where f_q [T^{-1}], f_e [T^{-1}], and f_o [T^{-1}] are the reverse TTDs of discharge via streams, evapotranspiration, and pumping.

[20] Nitrate transforms through denitrification (bacterial decomposition of organic matter under anoxic conditions) into gaseous forms [*Rivett et al.*, 2008]. The age distribution of water stored inside the catchment describes how long nitrate has been subject to denitrification. The volume of water within the saturated zone of the catchment is denoted by $S(t)$ [L^3]. The age distribution of $S(t)$ is denoted by $h(\tau,t)$ [T^{-1}] and is from here on referred to as the residence time distribution (RTD). It gives the fraction of $S(t)$ that entered at time $t - \tau$, where τ is the residence time of a parcel of water inside the saturated zone of the catchment. The RTD can be expressed as a function of the out-flowing water by

$$h(\tau, t) = \frac{1}{S(t)} \int_0^\infty f_q(\tau+\tau', t+\tau') Q(t+\tau') + f_e(\tau+\tau', t+\tau') \cdot E(t+\tau') + f_o(\tau+\tau', t+\tau') O(t+\tau') d\tau'. \tag{8}$$

[21] The deeper layers in the saturated zone have long travel times, while in the top of the saturated zone water moves fast and is constantly refreshed. This fast-flowing water, however, is only a small portion of the total storage and, consequently, has little influence on the RTD. In contrast, the out-flowing water is to a large extent influenced by these short travel times, particularly during high-discharge events. In summary, the RTD is expected to be relatively constant compared to the reverse TTD.

[22] Transient reverse TTDs for discharge and evapotranspiration were calculated by tracking particles through a groundwater flux field generated by MODFLOW [*McDonald and Harbaugh*, 1988]. The groundwater model, previously described by *van der Velde et al.* [2009], was extended to include the period of 1983–2008. The main characteristics of the groundwater model were a 5 × 5 m horizontal grid resolution, daily time steps, a single layer, year-round fixed surface water levels, a fixed effective storage coefficient to describe unsaturated zone effects, and a depth-dependent evapotranspiration reduction function. Note that although year-round fixed surface water levels were used, the surface water network was only allowed to drain water, not to supply water. Drainage occurred only when groundwater levels exceeded the surface water levels, creating an ephemeral draining surface water network. Transmissivity and effective storage of the groundwater model were manually adjusted to improve the simulation results for discharge and one groundwater head measurement location for years 1994 and 1995 (compared to the simulation results reported by *van der Velde et al.* [2009]). The model was validated for the years 1996–2001.

[23] To calculate transient reverse TTDs, every four MODFLOW model cells received one particle for every 20 mm of rainfall. Each particle therefore represented 2000 liters of water. The average discharge of the brook is 50 L s^{-1}, which translates into a daily outflow via discharge of approximately 2000 particles on average. The effective porosity was kept at 0.35 throughout the model.

[24] To simulate travel times longer than the runtime of the flow model, we used two modeled transient flux fields of 26 years consecutively and performed the particle tracking over 52 years. Only the last 26 years were analyzed; the first 26 years were needed to fill the storage of the model with particles and estimates of their travel time.

2.3.3. Solute Transport

[25] On its journey through the subsurface, a parcel of water exchanges chloride and nitrate with neighboring parcels by diffusion. It is assumed that chloride and nitrate do not react with the soil (no sorption or desorption). In the interest of model simplicity, we only consider the end result of diffusion by relating the concentration at the time a parcel leaves the saturated zone (through capillary upward flow or the groundwater-surface water interface) to the travel time; the concentration in the discharge thus depends on discharge time t and travel time T. *Botter et al.* [2005] showed that for complex catchment systems, with large soil heterogeneity and dense drainage networks, surface water quality could effectively be described by travel times without knowing the exact locations of water parcel travel paths. The concentration of a single parcel of water is denoted by $c(\tau,t)$ [$M\ L^{-3}$]. The concentration change of a parcel of water along its flow route before discharging ($\tau < T$), is described by

$$\frac{\partial c(\tau,t)}{\partial t} + \frac{\partial c(\tau,t)}{\partial \tau} = -r_n c(\tau,t) + r_d\big(C_{Eq}(\tau,t) - c(\tau,t)\big). \tag{9}$$

The first term on the right-hand side of equation (9) describes the decay of solutes (denitrification) with denitrification rate r_n [T^{-1}]. The second term describes the tendency of the parcel concentration to approach an equilibrium concentration, $C_{Eq}(\tau,t)$ [$M\ L^{-3}$] by diffusion and mixing. This process is controlled by the diffusion and mixing rate, r_d [T^{-1}]. Under complete mixing of the saturated zone, $C_{Eq}(\tau,t)$ has no spatial gradient along a travel path and is equal to the equilibrium concentration of the entire saturated zone $C_{Eq}(t)$. The spatial gradient of the water parcels concentration, $\partial c(\tau, t)/\partial\tau$, then is necessarily zero as well, and equation (9) reduces to

$$\frac{\partial c(\tau,t)}{\partial t} = -r_n c(\tau,t) + r_d\big(C_{Eq}(t) - c(\tau,t)\big), \tag{10}$$

where

$$C_{Eq}(t) = \frac{W_{sat}(t)}{S(t)}. \tag{11}$$

W_{sat} [M] is the total solute mass in the saturated zone, which can be obtained by a catchment-scale solute mass balance, and S [L^3] is the total water volume of the saturated zone. This approach was successfully applied for nitrate transport by *Rinaldo et al.* [2006] and *Botter et al.* [2008] for relatively short periods. However, long-term stream concentration records of nitrate in lowland catchments clearly show that lowland catchments are not completely mixed: during low discharge with long travel times, water parcels have low concentrations, while during average discharge with the associated average travel times, concentrations are much higher [e.g., *Rozemeijer and Broers*, 2007]. This indicates that not all travel times tend to the same equilibrium concentration and that the assumption of complete mixing will not suffice to describe the seasonal dynamics of nitrate transport.

[26] To accommodate a gradient in nitrate concentrations along a travel path caused by denitrification, we redefined the equilibrium concentration, $C_{Eq}(\tau,t)$, as the equilibrium concentration under average flow conditions after residence time τ. We also assumed that the equilibrium concentration as a function of residence time can be described by instantaneously redistributing all solute mass in the saturated zone. However, the solutes are not redistributed evenly over the saturated zone, but the redistribution follows an exponential decrease in concentration with increasing travel time describing the effect of denitrification. Although physically unrealistic, this last assumption allowed us to rewrite $C_{Eq}(\tau,t)$ as

$$C_{Eq}(\tau,t) = C_{Eq0}(t)e^{-r_n\tau}, \tag{12}$$

where C_{Eq0} is the equilibrium concentration for water parcels with zero travel time. Because $C_{Eq}(\tau,t)$ was defined as the equilibrium concentration of water parcels under average flow conditions (average storage $\overline{S}$ and average residence time distribution $\overline{h}$), $C_{Eq}(\tau,t)$ is also defined through

$$W_{sat}(t) = \overline{S}\int_0^\infty C_{Eq}(\tau,t)\overline{h}(\tau)\mathrm{d}\tau. \tag{13}$$

Combined with equation (12) this gives

$$C_{Eq}(\tau,t) = \frac{W_{sat}(t)}{\overline{S}\int_0^\infty \overline{h}(\tau')e^{-r_n\tau'}\mathrm{d}\tau'}e^{-r_n\tau}. \tag{14}$$

[27] Note that for chloride without decay ($r_n = 0$) equation (14) is almost equal to equation (11) but with a temporally averaged storage instead of a transient storage.

[28] The simplification of equation (9) into equation (10) is only allowed under complete mixing: $\partial c(\tau, t)/\partial\tau = 0$. By introducing equation (12), we violate this assumption. However, as long as $r_n \ll r_d$ (which ensures that the concentration of a water parcel is largely determined by denitrification when the concentration gradients between the equilibrium concentration and the concentration of the water parcel are small), this set of equations adequately approximates equation (9).

[29] Note that when the residence time is assumed to be a unique function of depth below the surface [*Raats*, 1977; *Broers*, 2004; *Broers and van Geer*, 2005], equation (14) implies that the saturated zone concentration is depth dependent. Similar concentration depth profiles were used by *Seibert et al.* [2009] to relate surface water concentrations at the point scale to groundwater concentrations in the riparian zone. However, by making the equilibrium concentration a function of residence time instead of the depth below the soil surface, it is possible to simulate more complex systems that do not have a clear relation between depth and travel time, such as systems with ephemeral active drainage areas and tube drainage.

[30] When we integrate equation (10) combined with equation (14) we obtain

$$C(T,t) = C_o(t-T)e^{-(r_d+r_n)T} + \frac{e^{-(r_d+r_n)T}}{\overline{S}\int_0^\infty \overline{h}(\tau)e^{-r_n\tau'}\mathrm{d}\tau'} \cdot \left(\int_0^T W_{sat}(t-T+\tau)e^{r_d\tau}\mathrm{d}\tau\right), \tag{15}$$

where C [$M\ L^{-3}$] is the concentration of water parcels leaving the catchment, and C_0 [$M\ L^{-3}$] is the starting concentration of a water parcel. This starting concentration is equal to the concentration of rainfall and is set to zero for both chloride and nitrate in this study. The catchment-scale mass balance of the solutes stored in the saturated zone is given by

$$\frac{dW_{sat}(t)}{dt} = J_{\text{leach}}(t) - J_{cap}(t) - J_Q(t) - r_n W_{sat}(t), \tag{16}$$

where J_{cap} [$M\ T^{-1}$] and J_Q [$M\ T^{-1}$] are the solute flux by capillary flow and stream discharge, respectively. The last term represents denitrification losses. The transfer function formulations of the solute fluxes leaving the saturated zone based on the reverse transfer function approach are

$$J_Q(t) = Q(t)\int_0^\infty f_q(T,t)C(T,t)\mathrm{d}T, \tag{17}$$

$$J_{cap}(t) = \max[(E(t)-P(t)),0]\int_0^\infty f_E(T,t)C(T,t)\mathrm{d}T. \tag{18}$$

Table 1. Calibrated Parameter Values and Estimated Parameter Ranges Used in the Sensitivity Analysis

Symbol	Definition	Range	Calibrated Value
r_d	Diffusion rate (day^{-1})	0.01–0.5[a]	0.20
$\overline{S_{rz}}$	Average water volume per area of the root zone (m)	0.05–0.15	0.093
Cu_{Cl}	Average chloride concentration of water taken up by plants (mg L^{-1})	5–20	9.7
u_{mN}	Mineral fraction of nitrate input	0.4–0.6	0.53
r_n	Denitrification rate (day^{-1})	1×10^{-4}–1×10^{-2}[a]	0.0025
r_m	Mineralization rate (day^{-1})	1×10^{-6}–1×10^{-4}[a]	6.7×10^{-5}
Cu_N	Average nitrate concentration of water taken up by plants (mg L^{-1})	150–350	261
a_f[b]	TTD "shift parameter"	−0.1 to 0.3[c]	0.0
a_h[b]	RTD "shift parameter"	−0.1 to 0.3[d]	0.0
Im_{Cl}[b]	Fertilizer chloride input multiplier	0.8–1.2	1.0
Im_N[b]	Fertilizer nitrate input multiplier	0.8–1.2	1.0
por[b]	Soil porosity → total average storage	0.3–0.45	0.35

[a]Parameter values are drawn from log-transformed ranges.
[b]These parameters are only used in the sensitivity analysis.
[c]Median travel time varies between 0.9 and 2.6 years; $a_f = 0$ corresponds to a median travel time of 1.8 years.
[d]Median residence time varies between 2.1 and 4 years; $a_h = 0$ corresponds to a median residence time of 3.1 years.

Travel times within the surface water are not considered, which limits this approach to small catchments with surface water travel times far smaller than the travel times through the saturated zone.

2.4. Calibration and Sensitivity Analysis of the Solute Transport Model

[31] First, we optimized the model parameters with the parameter estimation code PEST (J. Doherty, PEST Model-Independent Parameter Estimation, available at http://www.sspa.com/pest/download/pestman.pdf) on the entire nitrate and chloride stream concentration data set. For this calibration with a single objective function, we assumed no uncertainty in the parameters that resulted from the groundwater model (f_q, f_E, $\overline{h}$, and $\overline{S}$) and optimized the seven solute transport parameters (r_d, $\overline{S_{rz}}$, Cu_{Cl}, u_m, r_n, r_m, Cu_N). The rate of diffusion and mixing, r_d, and the average root zone water volume, $\overline{S_{rz}}$, were assumed to be equal for both nitrate and chloride. Via these two parameters the surface water chloride measurements could partly constrain the uncertainty in the nitrate mass balance. Plausible parameter ranges for all seven parameters were estimated from the literature and field experience [*Hassink*, 1992; *Schils and Kok*, 2003; *Haan and Skaggs*, 2003] and are given in Table 1. Furthermore, the yearly inputs of chloride and nitrate were allowed to vary within ranges of 0.8–1.2 times the estimated inputs (which were regional estimates). Note that the calibration of the yearly inputs only helps to explain the observed yearly fluctuations in stream concentration, but does not describe travel time related variations driven by seasonality and rainfall events (short-term concentration dynamics).

[32] We subdivided the model period into eight time intervals based on measurement type and frequency. For each of these intervals we not only calculated an average model error, Er, but also calculated the EAD, a measure that describes how well the model reproduces the temporal variations in surface water concentrations. The latter is derived from a plot showing the average difference between concentrations for five time-lag classes up to 1 month: 0–2 days, 2–5 days, 5–10 days, 10–20 days, and 20–30 days. We refer to this plot by "averaged difference plot," ADP (see Appendix A for a detailed derivation). For the calibration with PEST both error terms and an additional error term describing the difference between estimated and calibrated nitrate and chloride inputs were combined in an objective function. We refer to Appendix B for a detailed description of the error terms and the objective function we minimized with PEST.

[33] The uncertainty of the model results obtained by the optimized model and the parameter sensitivity were assessed by a global parameter sensitivity analysis of all parameters including the parameters that originated from the groundwater model. These parameters from the groundwater model (i.e., transient reverse TTD, the average RTD, and the average storage) were not recalculated because of excessive calculation times of the groundwater model. Instead, the sensitivity of the model to the calculated TTDs and RTD was evaluated by shifting the contributions of travel times within the distributions to larger contributions of younger or older water. The adjusted contribution of a certain travel or residence time was calculated by multiplying the original contribution with a shift factor, Um:

$$\mathrm{Um}(T,t) = \frac{\max\left[a\log\left(\frac{T}{\overline{T(t)}}\right)+1,\ 0\right]}{\int_0^\infty f(T,t)\max\left[a\log\left(\frac{T}{\overline{T(t)}}\right)+1,\ 0\right]\mathrm{d}T}, \qquad (19)$$

where a is the shift parameter that shifts the mean of the distribution (a_f for the reverse TTD, a_h for the RTD) and $\overline{T(t)}$ is the mean travel or residence time for time t. Positive a values correspond to an increase and negative values correspond to a decrease of the mean travel or residence time. The sensitivity of the model to the total average water storage in the saturated zone, $\overline{S}$, was evaluated by changing the soil porosity, "por." The sensitivity of the model to the inputs was evaluated by multiplying the calibrated inputs (PEST calibration) with a multiplication factor, Im. We randomly selected parameter sets from the ranges of Table 1 (uniform distributions). Models were designated "behavioral" when the average Er of the eight time intervals was less than 20%, the average EAD was less than 20%, and the R^2 was larger than 0.6. From 500 "behavioral" models the parameter correlations, the correlation between parameters

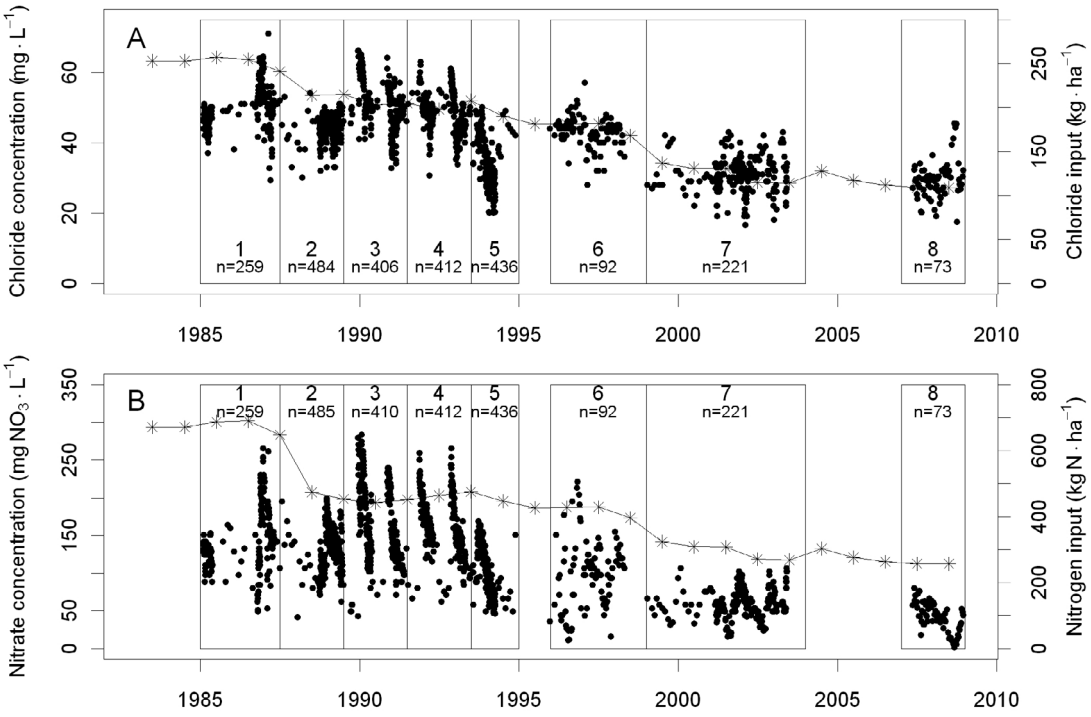

Figure 3. Concentrations of (a) chloride and (b) nitrate in the Hupsel Brook (dots) and estimated chloride and nitrogen fertilizer inputs (line). Boxes 1–8 represent the eight intervals into which the data set was subdivided during simulation, and *n* denotes the number of measurements each simulation period.

and model output, and the model output uncertainty as a result of parameter equifinality were analyzed.

[34] After calibration of the combined chloride and nitrate solute transport model with transient TTDs and evaluating the uncertainty of the calibrated solution caused by parameter equifinality [*Beven and Freer*, 2001], the optimal parameter set from the PEST calibration was used to run the same solute transport model with a time-averaged TTD. The time-averaged TTD is the flux-weighted average TTD for 26 years of calculated daily TTDs. This last calculation allowed us to assess the added value of transient TTDs over a single constant TTD.

3. Results and Discussion

3.1. Observed Surface Water Concentrations and Estimated Agricultural Inputs

[35] The data sets of estimated chloride and nitrate inputs from agriculture and measured surface water concentrations of the Hupsel Brook catchment are shown in Figure 3. The surface water concentrations of chloride and nitrate followed the decreasing trend in agricultural inputs. Both solutes also showed considerable seasonal and short-term fluctuations, with the latter related to individual rain events. The seasonal fluctuations of nitrate concentrations were larger than those of chloride. The nitrate concentration approached zero during summers, while the chloride concentration remained relatively high. We infer that, during low flows with long travel times, denitrification led to the observed low nitrate concentrations.

3.2. Flow Route Calculation by Groundwater Model and Particle Tracking

[36] Figure 4 shows the validation results of the groundwater model for the period 1996–2001. Good results were obtained for discharge and groundwater heads. The largest deviations between measured and predicted discharges between 500 and 5000 m^3 day^{-1} are mainly caused by a few events that were either missed or falsely predicted by the groundwater model.

[37] For every day during the model period of 26 years, a unique reverse TTD of the discharge was calculated by particle tracking through the transient flux field generated by the groundwater model. Figure 5 shows the results for an arbitrarily chosen wet (high discharge) day and a dry (low discharge) day. The logarithm of the travel time on the horizontal axis better reveals contributions of many different flow routes, each with characteristic time scales, than the travel time itself. Rainfall events in the past created the spiked shape of these outflow distributions: the reverse TTD will be zero for a travel time of *j* days if it did not rain *j* days ago. Particularly for relatively small travel times this produces pronounced spikes and "valleys" in the reverse TTD. The spiked behavior for short travel times averages out for longer travel times because the averaging classes to derive the distribution cover larger time intervals (they are equidistant in log time). With infinitely small classes the entire distribution would be spiked, reflecting contributions of all individual historical rainfall events.

[38] Figure 6a shows the reverse TTDs for every day during the entire model period with the values of the vertical axis of Figure 5a displayed in a color gradient. Vertical cross sections in Figure 6a give the reverse TTD of individual

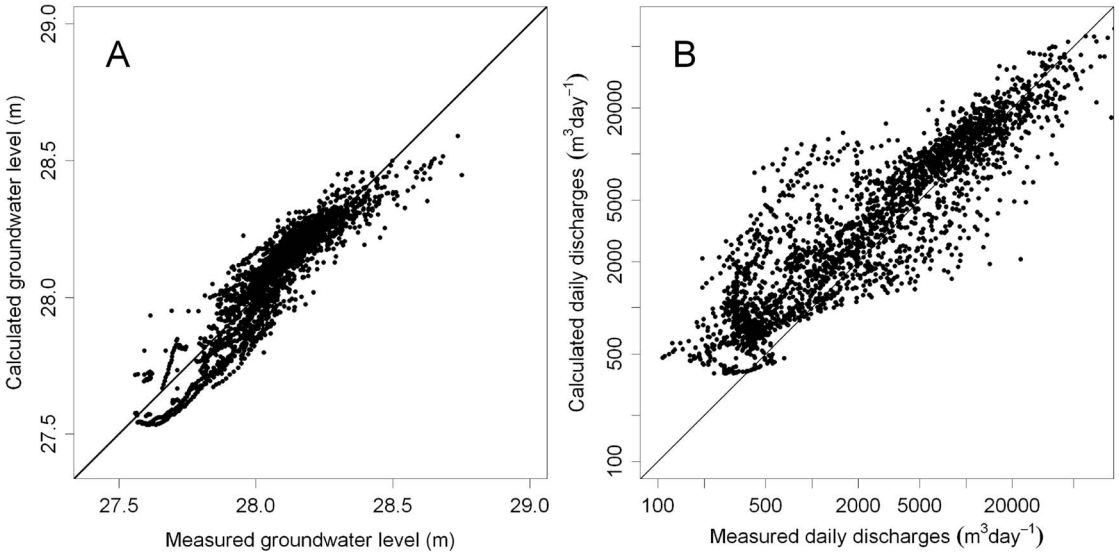

Figure 4. Validation results of the groundwater model for the period 1994–2001. (a) The results for a groundwater level measured at the meteorological station. (b) The results for the discharge at the catchment outlet.

days as given in Figures 5a and 5b. For any given day, Figure 6a gives the contribution of all rainfall events in the past to the discharge of that day. The effect of individual rain showers and dry periods that appear as spikes in Figure 5 appear in Figure 6a as bands that curve upward and to the right. Figure 6a shows that the individual spikes in Figures 5a and 5a belong to a complex structure of time-varying contributions of past rainfall events to the current discharge. The higher up in the graph, the longer ago the rainfall or drought event that caused the signal occurred. The curvature of the bands is caused by the logarithmic vertical scale. On a linear vertical scale the time-time space would create straight lines, but the detail for short travel times would be lost.

[39] Figure 6b gives the average discharge-weighted reverse TTD from 10% to 90%. The average daily median travel time is 1.8 years, with the 0.1 quantile of daily median travel times at 0.72 years and the 0.9 quantile at 2.74 years. The hump for short travel times (<10 days) represents contributions of fast flow routes, such as overland flow and tube drainage. Especially during high flow periods the fast flow routes (<10 days) contribute significantly to the reverse TTD.

3.3. Solute Transport Model Results

3.3.1. Calibration Results

[40] Simultaneous calibration of the chloride and nitrate transport model with PEST led to the optimal parameter set of Table 1. Figure 7 shows the simulation results for the eight selected time intervals, together with the observations. The behaviors of both chloride and nitrate are captured well by the model. Chloride in Figure 7 shows a slowly seasonally varying background concentration, with dilution during peak discharges. Nitrate shows more concentration variations than chloride. In many years, the nitrate concentration peaks in autumn during the first one or two discharge events. These peaks become less pronounced during the flushing season, during which most nitrates leached out of the catchment or were removed by denitrification.

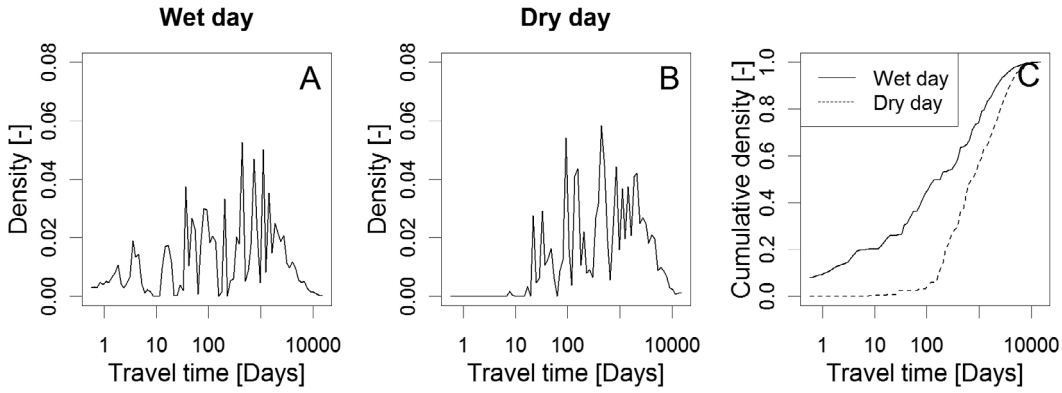

Figure 5. Reverse travel time distribution (TTD) for (a) a wet day and (b) a dry day and cumulative reverse TTDs for (c) both days.

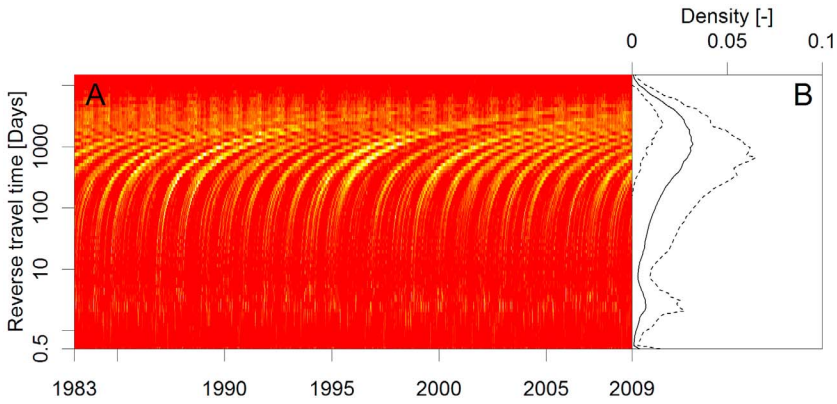

Figure 6. Daily reverse travel time distributions. (a) The color gradient indicates the density of the distribution (values of 0–0.1, dark to white). (b) The average (solid line) and 10% and 90% of daily densities around the average (dotted lines).

[41] The model performance was evaluated by the Er (relative absolute error), EAD (a dimensionless measure for temporal variation, Appendix B), and R^2 for each of the eight time intervals (Table 2). Overall satisfactory results for chloride and nitrate were obtained: Er values of around 8% for chloride and 12% for nitrate; R^2 values of around 0.65 for chloride and 0.70 for nitrate. The best results are obtained for periods with large concentration variations such as periods 2, 3, and 4.

[42] The averaged difference plots (ADPs) of all intervals show good agreement between measurements and simulations (Figure 8). This indicates that the nature of the observed temporal variations was well simulated by the model after calibration.

3.3.2. Mass Balance

[43] Table 3 gives the solute mass balance for each of the time intervals resulting from the PEST calibration. The results show that the mineral chloride storage was around 3 times the yearly input during the entire model period. The chloride storage decreased with decreasing inputs from 620 to 280 kg ha^{-1}. Stream discharge removed around 80% of the yearly chloride input. Plants took up an increasing percentage of yearly input starting around 20% in 1985 to almost 40% in 2008. This relative increase was mainly caused by the decreasing input.

[44] The model results show that nitrate storage in the organic reservoir of the root zone was very large (more than 20 times the yearly input). This is confirmed by a soil nitrogen survey on a 40 ha farm in the Hupsel Brook catchment in January 2006. An average soil nitrogen content of 2.3 g of N kg^{-1} dry soil was found. For an organic root zone of 35 cm this amounts roughly to 9×10^3 kg of N ha^{-1}. The decreasing N inputs during the last time intervals appeared to deplete the organic reservoir. Plant uptake remained relatively constant around 240 kg of N ha^{-1}. Variations in plant uptake are primarily a function of evapotranspiration, but especially during the last time intervals this uptake was only possible by decreasing the mineral and organic storage. The total mineral nitrate storage was around 1/3 of the yearly input, which is much less than the mineral storage for chloride. This difference is caused by denitrification of nitrate in the mineral phase. Between 25% and 40% of the yearly nitrogen input is removed by denitrification, and another 20% leaves the catchment by discharge.

3.3.3. Sensitivity Analysis

[45] The results of the sensitivity analysis are summarized in Figure 9. Behavioral nitrate simulations are sensitive to travel time (a_f), diffusion rate (r_d), and denitrification rate (r_n), while the chloride simulations are more sensitive to the uptake concentration of plants and the fertilizer inputs. The correlation between errors in simulated chloride concentrations of the surface water and the denitrification rate shows that the coupled chloride and nitrate calculation partly constrained the uncertainty in the calculated denitrification flux. The correlations between parameters (Figure 9b) reveal that travel time distributions are highly correlated with rate coefficients of diffusion and denitrification. This indicates that because both travel times and catchment-scale rate coefficients are uncertain and very difficult to measure; only the combination of travel time distributions with rate coefficients can be linked to measured concentrations. In Figure 7 the results of the behavioral runs for the stream concentration are indicated by the grey band around the solution found by PEST. The bandwidth of the behavioral solutions seems to increase with time. This is probably caused by decreasing inputs that lead to a relative increase in the contribution of mineralization as a source for nitrate in discharge. The organic storage and mineralization, however, have not been measured and are relatively uncertain.

[46] The high correlations between some parameters (Figure 9b) indicate model over-parameterization, which resulted in relatively large uncertainties for those fluxes and storages that could not be measured. The chloride input and the chloride uptake by plants, for example, have a strong negative correlation (Figure 9b), which implies that when

Figure 7. Stream water chloride and nitrate concentrations for each of the eight time intervals of Figure 3. The dots are the measurements. The solid line is the PEST simulation with transient reverse TTDs; the dashed line is the simulation with an average reverse TTD. The grey band envelopes the results of the "behavioral" runs from the sensitivity analysis. The bars at the bottom axis give an indication of the discharge at the catchment outlet (modeled).

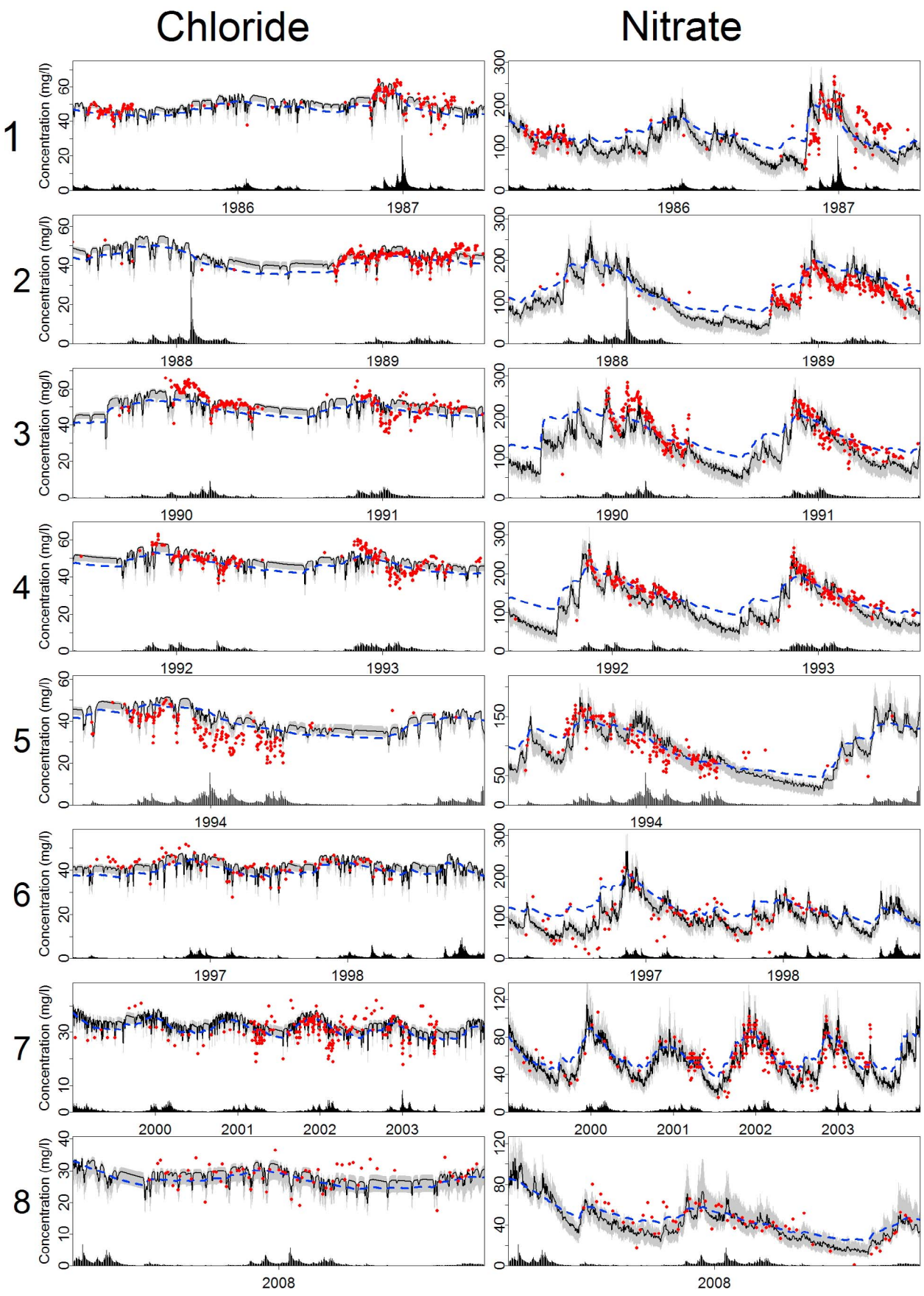
Chloride
Nitrate
1
2
3
4
5
6
7
8
Concentration (mg/l)
1986
1987
1988
1989
1990
1991
1992
1993
1994
1997
1998
2000
2001
2002
2003
2008

Figure 7

Table 2. Model Results After Calibration by PEST[a]

Period Number	Dates	Chloride			Nitrate		
		Er	EAD	R^2	Er	EAD	R^2
1	Jan 1983 to Jul 1987	0.04	0.06	0.71	0.17	0.25	0.43
2	Jul 1987 to Jul 1989	0.03	0.23	0.66	0.08	0.12	0.76
3	Jul 1989 to Jul 1991	0.05	0.17	0.62	0.11	0.14	0.77
4	Jul 1991 to Jul 1993	0.05	0.15	0.72	0.06	0.06	0.88
5	Jul 1993 to Jan 1996	0.15	0.27	0.65	0.13	0.22	0.69
6	Jan 1996 to Jan 1999	0.04	0.26	0.75	0.19	0.16	0.64
7	Jan 1999 to Jan 2007	0.08	0.29	0.49	0.11	0.14	0.70
8	Jan 2007 to Dec 2008	0.07	0.12	0.47	0.18	0.06	0.61
	Jan 1983 to Dec 2008	0.06	0.05	0.86	0.11	0.19	0.86

[a]Er is the mean error of the modeled concentration relative to the measured concentration (i.e., if the absolute values of the difference between measured and modeled concentration within a time period are, on average, 4% of the measured concentration, Er will be 0.04); EAD is the mean error of the modeled average difference plot relative to the measured average difference plot.

the uncertainty in at least one of these fluxes cannot be constrained by measurements, neither of them can be accurately determined.

[47] An indication for mass balance uncertainty is given in Table 3. In general, the uncertainty for the nitrate mass balance is larger than that for the chloride mass balance. Figure 9a shows that the results for chloride are most sensitive to the inputs and to plant uptake. As a consequence, only small ranges of possible chloride inputs yield a usable (behavioral) model, which results in a small uncertainty for the chloride inputs (Table 3). The nitrate results, however, are most sensitive to the travel times and reaction rate parameters that can compensate for input uncertainty. Hence, wide ranges of nitrate inputs can yield good models (depending on travel time and reaction rate parameters), and the uncertainties in nitrate input therefore remained relatively large. These uncertainties propagated to all other mass balance terms. The denitrification flux is the most uncertain flux with a coefficient of variation of 20%–40%. Evaluation of all behavioral runs showed that denitrification removed between 20% and 60% of the yearly input of nitrate and hence is a more dominant removal mechanism than surface water discharge (15%–35%) in the Hupsel Brook catchment.

3.3.4. Transient TTD Versus Constant TTD

[48] In Figure 7 we compare a model with transient reverse TTDs to a model with constant average reverse TTD (the mean reverse TTD of Figure 6b). It is clear that using transient instead of average reverse TTDs gives a much better representation of the dynamic nature of the solute concentrations.

[49] The dilution of chloride concentrations during peak discharges is not grasped by the model with a constant reverse TTD. Because the mass balance needs to be maintained, this model compensates for this by lowering the chloride concentration during low flow periods. During summer, discharge is relatively old. Due to more denitrification of nitrate in older water, the calculated nitrate concentrations during summer of the transient reverse TTD model are considerably lower than those of the constant reverse TTD model. The ADPs for chloride and nitrate in Figure 8 also clearly demonstrate that the model with transient reverse TTDs much better describes observed surface water concentration changes.

3.4. Implications for Travel Time Distributions

[50] Hydrologists have often tried to find smooth analytical approximations for TTDs based on stationary flow fields that could also describe the reaction of a catchment to rainfall [*Rinaldo et al.*, 2006; *Botter et al.*, 2008; *Lindgren et al.*, 2004]. In Figure 5 we show that travel time distributions are not smooth but spiked, reflecting rainfall and drought events during the journey of a water droplet. This spiked shape of transient reverse TTDs, in combination with significant contributions of long travel times in Figure 5a, shows that the Hupsel Brook catchment is able to discharge considerable amounts of old water during high discharge conditions [*Kirchner*, 2003] by rapidly increasing the active drainage area. Travel time distributions derived from unit hydrographs or from concentration input-output analysis describe the distribution of times it took the catchment to react to a rainfall event by discharge or stream concentration changes. These reaction time distributions do not describe

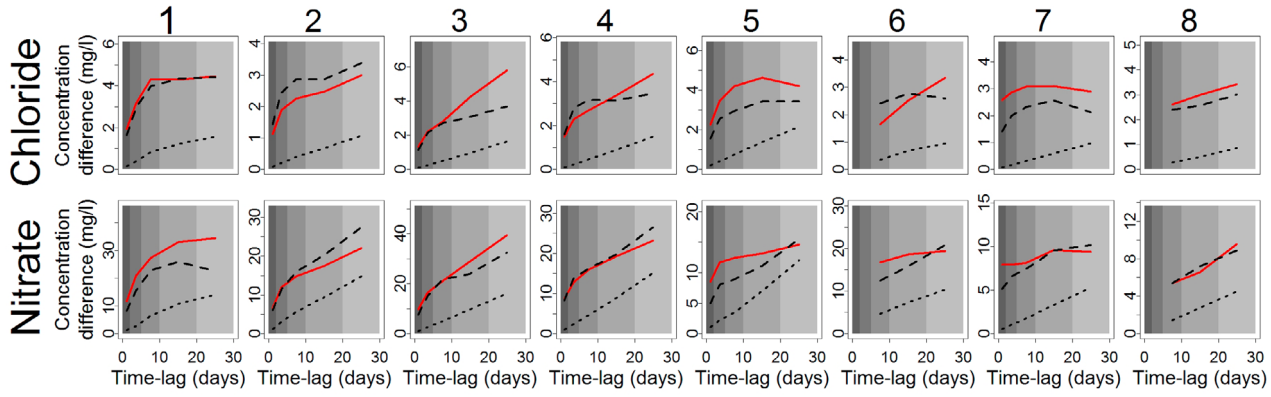

Figure 8. Average absolute difference plots (ADP; Appendix A) for the eight modeled time intervals (Figure 3) for chloride and nitrate. The five time-lag classes (0–2, 2–5, 5–10, 10–20, and 20–30 days) of the ADP are indicated by the five shades of grey. The average concentration difference for each time-lag class is indicated by the value of the lines in the center of the time-lag class. The measurements are represented by the solid line, the model with transient reverse TTDs is repesented by the dashed line, and the model with constant reverse TTD is represented by the dotted line.

Table 3. Mass Balances of Chloride and Nitrate for the Eight Simulated Time Intervals Calibrated by PEST[a]

	Time Interval							
	1	2	3	4	5	6	7	8
Chloride								
Yearly input (kg ha^{-1} yr^{-1})	229[b]	198[b]	187[b]	163[b]	186[b]	160[b]	141[b]	116[b]
Mineral storage (kg ha^{-1})	627[c]	575[c]	643[c]	611[c]	523[c]	528[c]	413[c]	355[c]
Total storage change (kg ha^{-1} yr^{-1})	8	7	7	−24	−61	−18	−11	−26
Removal by discharge (kg ha^{-1} yr^{-1})	182[b]	159[b]	146[b]	154[b]	209[b]	139[b]	112[b]	99[b]
Removal by plant uptake (kg ha^{-1} yr^{-1})	39[d]	33[d]	34[d]	33[d]	36[d]	39[d]	40[d]	43[d]
Nitrogen								
Yearly input (kg of N ha^{-1} yr^{-1})	639[c]	569[c]	518[c]	453[c]	412[c]	449[c]	276[c]	221[c]
Organic storage (kg of N ha^{-1})	9431[b]	9603[b]	9609[b]	9608[b]	9551[b]	9496[b]	9173[c]	8557[c]
Mineral storage (kg of N ha^{-1})	246[d]	277[c]	298[c]	269[c]	182[d]	234[c]	114[d]	82[d]
Total storage change (kg of N ha^{-1} yr^{-1})	100	59	−8	−53	−71	−55	−100	−147
Removal by discharge (kg of N ha^{-1} yr^{-1})	126[c]	132[b]	109[c]	115[c]	136[c]	96[c]	53[c]	46[c]
Removal by plant uptake (kg of N ha^{-1} yr^{-1})	240[d]	201[d]	208[d]	201[d]	219[d]	240[d]	243[c]	261[c]
Removal by denitrification (kg of N ha^{-1} yr^{-1})	173[d]	177[d]	209[d]	189[d]	126[d]	168[d]	79[d]	61[d]

[a]Indications of the uncertainty of the mass balance terms based on the sensitivity analyses are added in superscript.
[b]Standard deviation "behavioral runs" less than 10% of mean value.
[c]Standard deviation "behavioral runs" less than 20% of mean value.
[d]Standard deviation "behavioral runs" less than 40% of mean value.

the actual contact times and travel paths of water parcels through the soil, which are the important characteristics for solute transport. The spiked reverse TTDs presented in Figure 5 do describe the distribution of contact times between rainwater and soil, while also being transfer functions to transfer discharge into historic rainfall (equation (7)). From the many spikes in the reverse TTDs of Figure 5 it is clear that the transient reverse TTDs cannot simply be inverted from hydrographs or from concentration time series, and more research is needed to unravel their controls.

[51] The mixing of waters with different ages explains how a catchment is able to control the chemistry of discharge [*Kirchner*, 2003]. The surface water concentration is a result of mixing of a large volume of old water with a relatively constant concentration with a discharge-dependent contribution of younger water with variable concentrations. This leads to clear relations between discharge and concentration. Consequently, for water quality purposes it is more relevant to know the contributions of relatively young water to discharge than to know the average catchment travel time.

3.5. Catchment Behavior and Model Limitations

[52] The catchment-scale mineralization rate for nitrate resulting from the calibration (Table 1) is slightly lower than rates found by *Hassink* [1992], who found mineralization rates between 2×10^{-4} and 5×10^{-4} day^{-1} for Dutch sandy soils in laboratory incubation tests at 25°C. Our rate, however, represents field conditions with an average yearly temperature of around 10°C (at 25°C our rate is multiplied by 2.5). Not many regional denitrification rates have been published. More importantly, we expect these rates to be

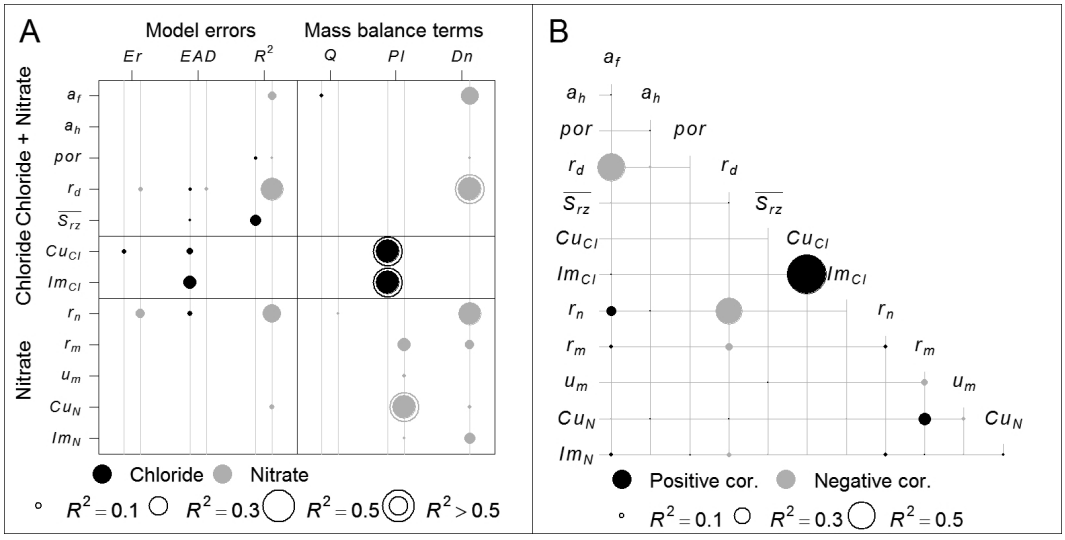

Figure 9. Sensitivity and correlation analysis of the 12 model parameters describing chloride and nitrate transport. (a) The sensitivity of the model errors to the parameters and the correlations between parameters and three selected mass balance terms for both chloride and nitrate: *Q*, removal by discharge; Pl, removal by plant uptake; Dn, removal by denitrification. (b) The correlations between parameters. Only correlations larger than 5% are shown. A distinction is made between positive and negative correlations.

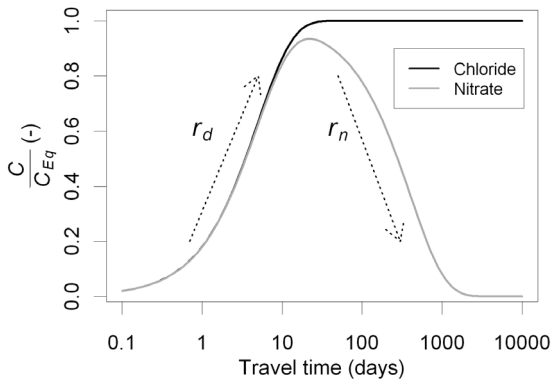

Figure 10. Concentrations of chloride and nitrate relative to a constant equilibrium concentration, C_{Eq}, in a water parcel traveling through the subsurface as function of travel time. The diffusion rate r_d determines the influx of solutes in an initially solute-free water parcel, while r_n is the denitrification rate of the nitrate in a water parcel.

highly dependent on local aquifer properties such as dissolved organic carbon concentrations, pyrite concentrations, and thickness and heterogeneity of the top aquifer [*Zhang et al.*, 2009]. The mineral fraction of yearly applied nitrogen fertilizer of 53% compares well to the ratios of applied manure in the study of *Schils and Kok* [2003].

[53] The effect of the model parameters r_d and r_n on chloride and nitrate response is visualized in Figure 10 for a solution of equation (15) with a constant equilibrium concentration in the saturated zone, $\overline{C_{Eq}}$. Chloride reaches its maximum concentration after a travel time in the saturated zone of around 20 days, while the nitrate concentration peaks after about 20 days and then gradually drops off as denitrification becomes more effective.

[54] From Figure 10 we conclude that the observed dilution of chloride concentrations during high discharge events (Figure 7) stems from travel times shorter than 20 days, which is the contribution of fast flow routes. The hub during short travel times in Figure 6b shows the average contribution of short travel times to the total reverse TTD. However, calculations of the contributions of short travel times to the discharge are very uncertain and sensitive to the chosen porosity and cell size.

[55] According to Figure 10, the nitrate concentration peaks for travel times around 20 days. The resulting temporal variation of surface water concentrations is much larger for nitrate than for chloride (Figure 7). Figure 7 also warrants the conclusion that a constant travel time distribution is useful to evaluate the long-term mass balance of a solute, but if we want to relate measured surface water concentrations to model simulations, we need to incorporate the dynamic mixing of waters with different travel times via transient travel time distributions.

[56] The sensitivity analysis showed that the calibrated optimal solution is a plausible solution, but that uncertainties are large, particularly in the denitrification flux and plant uptake of chloride and nitrate. Because the catchment-scale diffusion, denitrification, and mineralization rate parameters will always need calibration, stream concentration measurements can only constrain the uncertainty of the combined results for travel times and rate parameters, but not for the separate parameters. Additional measurements of organic nitrogen storage and plant uptake of nitrate would help to create a more reliable catchment-scale mass balance but will not necessarily lead to a better model for the stream concentrations.

3.6. Model Evaluation

[57] We, intentionally, did not divide the measured data set into a calibration and validation period. Our aim was to use the model to interpret the observed concentrations of nitrate and chloride, analyzing which part of the observed concentration variations can be attributed to overall mass balance changes and which part to travel time variations. Furthermore, the model was used to quantify the nitrate fluxes by plant uptake, denitrification, and stream discharge at the catchment scale and to evaluate to what extent the uncertainty in these fluxes could be constrained by simultaneously calculating the chloride and nitrate fluxes. Excluding part of the measurements for a separate model validation would not improve our understanding of the inner workings of the catchment and instead would increase the uncertainty of the model results.

[58] The advantage of particle tracking combined with mass transfer functions over a fully coupled spatially distributed flow and transport model is the limited number of parameters that are needed to describe the solute transport by water parcels. The latter allowed us to create a very detailed groundwater flow model that focuses on the representation of tube drains and small ditches. This proved necessary to calculate the contributions of relatively short travel times that influence the surface water concentration most. The solute transport description by mass transfer functions allowed us to run the solute transport part of the model thousands of times so that catchment-scale solute transport parameters could be calibrated and sensitivity and uncertainty analyses could be performed. Furthermore, the proposed model setup reflected the available information: abundant information on topography and soil hydraulic properties and little information on the solute transport characteristics of soils and solute input.

4. Conclusions

[59] We developed a model that describes daily chloride and nitrate concentrations with a single set of parameters for a period of 26 years. By assuming that the parameters that describe diffusive and convective transport are the same for chloride and nitrate, we were able to partly constrain the uncertainty in the unknown nitrate flux caused by denitrification. We estimated that denitrification removed between 20% and 60% of the yearly inputs, while stream discharge removed between 15% and 35%. These estimates take into account all parameter uncertainties and show that far more nitrate leaves the catchment by denitrification than by surface water discharge. The long-term trend of decreasing chloride and nitrate concentrations at the outlet of the 6.6 km^2 Hupsel Brook catchment originated from two decades of decreasing agricultural inputs. More rapid concentration fluctuations (seasonal and daily) were shown to arise from variations in groundwater travel times that were directly linked to temporal precipitation patterns.

[60] Our results demonstrated that observed chloride and nitrate concentration dynamics cannot be solely explained

from time series of discharge, rainfall, and solute inputs, but that the dynamics in contact times of water parcels with the soil, expressed by transient reverse travel time distributions (TTDs), are essential for understanding observed concentration dynamics. To calculate transient reverse TTDs successfully, an adequate representation of the strongly ephemeral character of the surface water network was paramount. We showed that transient TTDs do not have the smooth shape they are often ascribed in the literature, but that they are spiked, reflecting precipitation and evapotranspiration periods. Especially for small catchments like the Hupsel Brook catchment with a relatively large proportion of fast flow routes and short travel times, large variances in travel time distributions can be expected. Therefore, hydrological models used for solute transport should not just describe the reaction of stream discharge or stream concentration on rainfall events. Instead, the models should focus on the dynamics of travel times and travel path of water parcels within a catchment.

Appendix A: Average Absolute Difference Plot

[61] We characterized the temporal variation of stream water concentrations by an average absolute difference plot (ADP). We defined five time-lag classes up to 1 month: 0–2 days, 2–5 days, 5–10 days, 10–20 days, and 20–30 days, and calculated a mean absolute concentration change for pairs of concentrations within each time-lag class. The resulting averaged differences can be plotted for the different lag classes in an ADP. The ADP is calculated by

$$\mathrm{AD}(l) = \frac{1}{\|N(l)\|} \sum_{(t_1,t_2)\in N(l)} |C(t_2) - C(t_1)|, \tag{A1}$$

where AD(l) is the average absolute concentration difference within time-lag class l. $N(l)$ is the set of data pairs within class l, and $\|N(l)\|$ is the number of data pairs. The measured or modeled concentration is denoted by C. We chose the ADP method over the more commonly used correllogram, because the ADP deals more easily with uneven sampling intervals of concentration measurements and because the unit of the ADP (concentration) compares better to the mean absolute concentration error in the calibration object function.

Appendix B: Calibration Specifications

[62] We calibrated the solute transport model by minimizing the sum of three error terms. The first error term, Er, describes the mean absolute error. The second error term, EAD, describes the deviation between the ADP of the measurements and the model, and the last error term describes the deviation of the calibrated nitrate and chloride inputs from the estimated inputs.

[63] The relative mean absolute error between model and measurements is calculated by

$$\mathrm{Er}_{i,p} = \frac{\sum_{t=1}^{n_p} \left| C_{q,i}(t) - C_{m,i}(t) \right|}{\sum_{t=1}^{n_p} C_{m,i}(t)}, \tag{B1}$$

where subscript i denotes chloride (i = Cl) or nitrate (i = N) and p denotes the time interval. The modeled concentration is denoted by C_q, and the measured concentration is denoted by C_m. The number of measurements within an interval is given by n_p.

[64] We compared the ADP of the measurements with that of the model at all measurement times. For perfect measurements and a perfect model, both ADPs should be equal. However, to account for measurement errors (due to the sampling strategy, laboratory analyses, and sample transportation and handling), an estimate of the measurement error is subtracted from the ADP of the measurements. We arbitrarily defined the measurement error as 25% of the mean absolute difference of the first time-lag class (lag times up to 2 days when available, otherwise the first lag class available). The ADP differences between measurements and model are valued by

$$\mathrm{EAD}_{i,p} = \frac{1}{5}\sum_{l=1}^{5}\left(\frac{\mathrm{AD}_{mod,i,p}(l) - \left(\mathrm{AD}_{meas,i,p}(l) - 0.25\mathrm{AD}_{meas,i,p}(1)\right)}{\mathrm{AD}_{meas,i,p}(l) - 0.25\mathrm{AD}_{meas,i,p}(1)}\right), \tag{B2}$$

where $\mathrm{AD}_{mod}(l)$ is the average difference of the modeled concentrations with time lags within class l while $\mathrm{AD}_{meas}(l)$ is the corresponding averaged difference of the observed concentrations. An estimate for the measurement error is given by $0.25\mathrm{AD}_{meas}(1)$ as indicated above.

[65] Because we also calibrated the yearly fertilizer input, the number of calibration parameters was rather large. We reduced the consequent risk of nonuniqueness by introducing an extra error term, EF. This term allows for deviations from the estimated input, but also guides the calibration toward an input value as close as possible to the estimated input:

$$\mathrm{EF}_{i,p} = \left(1 - \frac{\mathrm{Fcal}_{i,p}}{\mathrm{Fest}_{i,p}}\right)^2, \tag{B3}$$

where Fcal [$M\ T^{-1}$] is the calibrated estimated fertilizer rate and Fest is the regional estimated fertilizer rate.

[66] The objective function, Obj, that was minimized to find an optimal solution is given by

$$\begin{aligned}\mathrm{Obj} = {} & w_1\left(\sum_{p=1}^{8}\mathrm{Er}_{\mathrm{Cl},p} + \sum_{p=1}^{8}\mathrm{Er}_{\mathrm{N},p}\right) \\ & + w_2\left(\sum_{p=1}^{8}\mathrm{EAD}_{\mathrm{Cl},p} + \sum_{p=1}^{8}\mathrm{EAD}_{\mathrm{N},p}\right) \\ & + w_3\left(\sum_{p=1}^{8}\mathrm{EF}_{\mathrm{Cl},p} + \sum_{p=1}^{8}\mathrm{EF}_{\mathrm{N},p}\right),\end{aligned} \tag{B4}$$

where $w_{1,\ldots,3}$ are the weighting factors for the individual error terms. These weighting factors were determined by performing several calibration runs that minimize equation (B4), until the individual error terms contributed 5:2:1 to Obj, reflecting the importance of each of the error terms.

[67] We further improved this calibration by two data corrections: excluding concentration measurements taken during the 10% lowest flows and excluding the 2% largest

deviations between measured and modeled solute concentrations. The first correction excluded measurements during periods with long surface water residence times. Plant uptake and stream bed denitrification at those times are important extra loss terms that blur the comparison between measurements and model results. Furthermore, during dry conditions only a small part of the main brook drains water that reaches the catchment outlet. The transport characteristics of this part of the catchment deviate from those of the catchment as a whole (caused by a locally sandier and thicker aquifer). For these reasons we considered it undesirable to calibrate a solute transport model for the entire catchment on measurements taken during low flows. The second correction reduces the impact of any large measurement errors or of discharge peaks that were wrongly predicted by the groundwater model.

[68] **Acknowledgments.** The authors are grateful to Piet Warmerdam and Jacques Kole of Wageningen University for collecting and sharing the extensive hydrological data set of the Hupsel Brook catchment. This study has been made possible by the financial support of TNO, Deltares, and Alterra. The comments of three anonymous reviewers were of great value for improving this paper.

References

Beven, K. J., and J. Freer (2001), Equifinality, data assimilation, and uncertainty estimation in mechanistic modelling of complex environmental systems using the GLUE methodology, *J. Hydrol.*, *249*, 11–29.

Botter, G., E. Bertuzzo, A. Bellin, and A. Rinaldo (2005), On the Lagrangian formulations of reactive solute transport in the hydrologic response, *Water Resour. Res.*, *41*, W04008, doi:10.1029/2004WR003544.

Botter, G., E. Peratoner, M. Putti, A. Zuliani, R. Zonta, A. Rinaldo, and M. Marani (2008), Observation and modeling of catchment-scale solute transport in the hydrologic response: A tracer study, *Water Resour. Res.*, *44*, W05409, doi:10.1029/2007WR006611.

Botter, G., E. Milan, E. Bertuzzo, S. Zanardo, and A. Rinaldo (2009), Inference from catchment-scale tracer circulation experiments, *J. Hydrol.*, *369*, 368–380.

Botter, G., E. Bertuzzo, and A. Rinaldo (2010), Transport in the hydrologic response: Travel time distributions, soil moisture dynamics, and the old water paradox, *Water Resour. Res.*, *46*, W03514, doi:10.1029/2009WR008371.

Broers, H. P. (2004), The spatial distribution of groundwater age for different geohydrological situations in the Netherlands: Implications for groundwater quality monitoring at the regional scale, *J. Hydrol.*, *299*, 84–106.

Broers, H. P., and F. C. van Geer (2005), Monitoring strategies at phreatic wellfields: A 3D travel time approach, *Ground Water*, *43*, 850–862.

Cardenas, M. B. (2007), Potential contribution of topography-driven regional groundwater flow to fractal stream chemistry: Residence time distribution analysis of Tóth flow, *Geophys. Res. Lett.*, *34*, L05403, doi:10.1029/2006GL029126.

Cardenas, M. B. (2008), Surface water-groundwater interface geomorphology leads to scaling of residence times, *Geophys. Res. Lett.*, *35*, L08402, doi:10.1029/2008GL033753.

Ernst, L. F. (1978), Drainage of undulating sandy soils with high groundwater tables, *J. Hydrol.*, *39*, 1–30.

Haan, P. K., and R. W. Skaggs (2003), Effect of parameter uncertainty on DRAINMOD predictions: II. Nitrogen loss, *Am. Soc. Agric. Eng.*, *46*, 1069–1075.

Hassink, J. (1992), Effects of soil texture and structure on carbon and nitrogen mineralization in grassland soils, *Biol. Fertil. Soils*, *14*, 126–134.

Hassink, J., L. A. Bouwman, K. B. Zwart, J. Bloem, and L. Brussaard (1993), Relationships between soil texture, physical protection of organic matter, soil biota, and C and N mineralization in grassland soils, *Geoderma*, *57*, 105–128.

Herlihy, M. (1979), Nitrogen mineralization in soils of varying texture, moisture and organic matter. I. Potential and experimental values in fallow soils, *Plant Soil*, *53*, 255–267.

Hopmans, J. W., and J. N. M. Stricker (1989), Stochastic analysis of soil water regime in a watershed, *J. Hydrol.*, *105*, 57–84.

Kirchner, J. W. (2003), A double paradox in catchment hydrology and geochemistry, *Hydrol. Processes*, *17*, 871–874.

Kirchner, J. W., X. Feng, and C. Neal (2000), Fractal stream chemistry and its implications for contaminant transport in catchments, *Nature*, *403*, 524–527.

Kollet, S. J., and R. M. Maxwell (2008), Demonstrating fractal scaling of baseflow residence time distributions using a fully-coupled groundwater and land surface model, *Geophys. Res. Lett.*, *35*, L07402, doi:10.1029/2008GL033215.

Kollet, S. J., R. M. Maxwell, C. S. Woodward, S. Smith, J. Vanderborght, H. Vereecken, and C. Simmer (2010), Proof of concept of regional scale hydrologic simulations at hydrologic resolution utilizing massively parallel computer resources, *Water Resour. Res.*, *46*, W04201, doi:10.1029/2009WR008730.

Lindgren, G. A., G. Destouni, and A. V. Miller (2004), Solute transport through the integrated groundwater-stream system of a catchment, *Water Resour. Res.*, *40*, W03511, doi:10.1029/2003WR002765.

Makkink, G. F. (1957), Testing the Penman formula by means of lysimeters, *J. Int. Water Eng.*, *11*, 277–288.

McDonald, M. G., and A. W. Harbaugh (1988), A modular three dimensional finite-difference ground-water flow model,*U.S. Geol. Surv. Tech. Water Resour. Invest.*, *Book 6*, *Chap. A1*, 586 pp. (Available at http://pubs.water.usgs.gov/twri6a1.)

Petrolia, D. R., and P. H. Gowda (2006), Missing the boat: Midwest farm drainage and Gulf of Mexico hypoxia, *Rev. Agric. Econ.*, *28*, 240–253.

Raats, P. A. C. (1977), Convective transport of solutes by steady flows. I. General theory, *Agric. Water Manage.*, *1*, 201–218.

Rinaldo, A., and M. Marani (1987), Basin scale model of solute transport, *Water Resour. Res.*, *23*, 2107–2118.

Rinaldo, A., A. Bellin, and M. Marani (1989), A study on solute NO_3-N transport in the hydrologic response by an MRF model, *Ecol. Modell.*, *48*, 159–191.

Rinaldo, A., G. Botter, E. Bertuzoo, A. Ucelli, T. Settin, and M. Marani (2006), Transport at basin scales: 1. Theoretical framework, *Hydrol. Earth Syst. Sci.*, *10*, 19–29.

Rivett, M. O., S. R. Buss, P. Morgan, J. W. N. Smith, and C. D. Bemment (2008), Nitrate attenuation in groundwater: A review of biogeochemical controlling processes, *Water Res.*, *42*, 4215–4232.

Rodrigo, A., S. Recous, C. Neel, and B. Mary (1997), Modelling temperature and moisture effects on C-N transformations in soils: comparison of nine models, *Ecol. Modell.*, *102*, 325–339.

Rozemeijer, J. C., and H. P. Broers (2007), The groundwater contribution to surface water contamination in a region with intensive agricultural land use (Noord-Brabant, The Netherlands), *Environ. Pollut.*, *148*, 695–706.

Schils, R. L. M., and I. Kok (2003), Effects of cattle slurry manure management on grass yield, *Neth. J. Agric. Sci.*, *51*(1–2), 41–65.

Seibert, J., T. Grabs, S. Köhler, H. Laudon, M. Winterdahl, and K. Bishop (2009), Linking soil- and stream-water chemistry based on a Riparian Flow-Concentration Integration Model, *Hydrol. Earth Syst. Sci.*, *13*, 2287–2297.

Sivapalan, M. (2003), Process complexity at hillslope scale, process simplicity at the watershed scale: is there a connection?, *Hydrol. Processes*, *17*, 1037–1041.

van den Eerthwegh, G. A. P. H., and C. R. Meinardi (1999), Water—En nutrientenhuishouding van het stroomgebied van de Hupselse beek (in Dutch), Wageningen Univ., Wageningen, Netherlands.

van der Molen, D. T., R. Portielje, W. T. de Nobel, and P. C. M. Boers (1998), Nitrogen in Dutch freshwater lakes: trends and targets, *Environ. Pollut.*, *102*, 553–557.

van der Velde, Y., G. H. de Rooij, and P. J. J. F. Torfs (2009), Catchment-scale non-linear groundwater-surface water interactions in densely drained lowland catchments, *Hydrol. Earth Syst. Sci.*, *13*, 1867–1885.

van der Velde, Y., J. C. Rozemeijer, G. H. de Rooij, F. C. van Geer, and H. P. Broers (2010), Field-scale measurements for separation of catchment discharge into flow route contributions, *Vadose Zone J.*, *9*, 25–35, doi:10.2136/vzj2008.0141.

van Ommen, H. C., R. Dijksma, J. M. H. Hendrickx, L. W. Dekker, J. Hulshof, and M. van den Heuvel (1989), Experimental assessment of preferential flow paths in a field soil, *J. Hydrol.*, *105*, 253–262.

Visser, A., H. P. Broers, R. Heerdink, M. F. P. Bierkens (2009), Trends in pollutant concentrations in relation to time of recharge and reactive transport at the groundwater body scale, *J. Hydrol.*, *369*, 427–439.

Wösten, J. H. M., J. Bouma, and G. H. Stoffelsen (1985), Use of soil survey data for regional soil water simulation models, *Soil Sci. Soc. Am. J.*, *49*, 1238–1244.

Wriedt, G., J. Spindler, T. Neef, R. Meißner, and M. Rode (2007), Groundwater dynamics and channel activity as major controls of in-stream nitrate concentrations in a lowland catchment system?, *J. Hydrol.*, *343*, 154–168.

Zhang, Y.-C., C. P. Slomp, H. P. Broers, H. F. Passier, and P. van Cappellen (2009), Denitrification coupled to pyrite oxidation and changes in groundwater quality in a shallow sandy aquifer, *Geochim, Cosmochim. Acta*, *73*, 6716–6726.

H. P. Broers, Deltares, PO Box 85467, NL-3508 AL Utrecht, Netherlands.

G. H. de Rooij, Department of Soil Physics, Helmholtz Centre for Environmental Research-UFZ, Theodor-Lieser-Strasse 4, D-06120 Halle, Germany.

J. C. Rozemeijer and F. C. van Geer, Department of Physical Geography, Utrecht University, PO Box 80115, NL-3508 TC Utrecht, Netherlands.

Y. van der Velde, Soil Physics, Ecohydrology and Groundwater Management Group, Wageningen University, PO Box 47, NL-6700 AA Wageningen, Netherlands. (ype.vandervelde@wur.nl)